

1 **High-order cognition is supported by complex but**
2 **compressible brain activity patterns**

3 Lucy L. W. Owen^{1,2} and Jeremy R. Manning^{1,*}

4 ¹Department of Psychological and Brain Sciences,
5 Dartmouth College, Hanover, NH

6 ²Carney Institute for Brain Sciences,
7 Brown University, Providence, RI

8 *Address correspondence to jeremy.r.manning@dartmouth.edu

9 February 28, 2023

10 **Abstract**

11 We applied dimensionality reduction algorithms and pattern classifiers to functional neu-
12 roimaging data collected as participants listened to a story, temporally scrambled versions of
13 the story, or underwent a resting state scanning session. These experimental conditions were
14 intended to require different depths of processing and inspire different levels of cognitive en-
15 gagement. We considered two primary aspects of the data. First, we treated the number of
16 features (components) required to achieve a threshold decoding accuracy as a proxy for the
17 “compressibility” of the neural patterns (where fewer components indicate greater compres-
18 sion). Second, we treated the maximum achievable decoding accuracy across participants as
19 an indicator of the “stability” of the recorded patterns. Overall, we found that neural patterns
20 recorded as participants listened to the intact story required fewer features to achieve compa-
21 rable classification accuracy to the other experimental conditions. However, the peak decoding
22 accuracy (achievable with more features) was also highest during intact story listening. Taken
23 together, our work suggests that our brain networks flexibly reconfigure according to ongoing
24 task demands, and that the activity patterns associated with higher-order cognition and high
25 engagement are both more complex and more compressible than the activity patterns associated
26 with lower-order tasks and lower levels of engagement.

27 **Keywords:** information, compression, temporal decoding, dimensionality reduction, neu-
28 roimaging

29 **Introduction**

30 Large-scale networks, including the human brain, may be conceptualized as occupying one or
31 more positions along on a continuum. At one extreme, every node is fully independent of every
32 other node. At the other extreme, all nodes behave identically. Each extreme optimizes key
33 properties of how the network functions. When every node is independent, the network is

29 maximally *expressive*: if we define the network’s “state” as the activity pattern across its nodes,
30 then every state is equally reachable by a network with fully independent nodes. On the other
31 hand, a network of identically behaved nodes optimizes *robustness*: any subset of nodes may
32 be removed from the network without any loss of function or expressive power, as long as any
33 single node remains. Presumably, most natural systems tend to occupy positions between these
34 extremes. We wondered: might the human brain reconfigure itself to be more flexible or more
35 robust according to ongoing demands? In other words, might the brain reconfigure its connections
36 or behaviors under different circumstances to change its position along this continuum?

37 Closely related to the above notions of expressiveness versus robustness are measures of
38 how much *information* is contained in a given signal or pattern, and how *redundant* a signal
39 is (Shannon, 1948). Formally, information is defined as the amount of uncertainty about a given
40 variables’ outcomes (i.e., entropy), measured in *bits*, or the optimal number of yes/no questions
41 needed to reduce uncertainty about the variable’s outcomes to zero. Highly complex systems with
42 many degrees of freedom (i.e., high flexibility and expressiveness), are more information-rich than
43 simpler or more constrained systems. The redundancy of a signal denotes the difference how
44 expressive the signal *could* be (i.e., proportional to the number of unique states or symbols used
45 to transmit the signal) and the actual information rate (i.e., the entropy of each individual state or
46 symbol). If a brain network’s nodes are fully independent, then the number of bits required to
47 express a single activity pattern is proportional to the number of nodes. The network would also
48 be minimally redundant, since the status of every node would be needed to fully express a single
49 brain activity pattern. If a brain network’s nodes are fully coupled and identical, then the number
50 of bits required to express a single activity pattern is proportional to the number of unique states
51 or values any individual node can take on. Such a network would be highly redundant, since
52 knowing any individual node’s state would be sufficient to recover the full-brain activity pattern.
53 Highly redundant systems are also robust, since there is little information loss from losing any
54 given observation.

55 We take as a given that brain activity is highly flexible: our brains can exhibit nearly infinite ac-
56 tivity patterns. This flexibility implies that our brains activity patterns are highly information rich.
57 However, brain activity patterns are also highly structured. For example, full-brain correlation
58 matrices are stable within (Finn et al., 2015, 2017; Gratton et al., 2018) and across (Yeo et al., 2011;

59 Gleerean et al., 2012; Gratton et al., 2018; Cole et al., 2014) individuals. This stability suggests that
60 our brains' activity patterns are at least partially constrained, for example by anatomical, external,
61 or internal factors. Constraints on brain activity that limit its flexibility decrease expressiveness
62 (i.e., its information rate). However, constraints on brain activity also increase its robustness to
63 noise (e.g., “missing” or corrupted signals may be partially recovered). For example, recent work
64 has shown that full-brain activity patterns may be reliably recovered from only a relatively small
65 number of implanted electrodes (Owen et al., 2020; Scangos et al., 2021). This robustness property
66 suggests that the relevant signal (e.g., underlying factors that have some influence over brain
67 activity patterns) are compressible.

68 To the extent that brain activity patterns contain rich task-relevant information, we should
69 be able to use the activity patterns to accurately differentiate between different aspects of the
70 task (e.g., using pattern classifiers; Norman et al., 2006). For example, prior work has shown a direct
71 correspondence between classification accuracy and the information content of a signal (Alvarez,
72 2002). To the extent that brain activity patterns are compressible, we should be able to generate
73 simplified (e.g., lower dimensional) representations of the data while still preserving the relevant
74 or important aspects of the original signal. In general, information content and compressibility are
75 related but are partially dissociable (Fig. 1). If a given signal (e.g., a representation of brain activity
76 patterns) contains more information about ongoing cognitive processes, then the peak decoding
77 accuracy should be high. And if the signal is compressible, a low-dimensional embedding of the
78 signal will be similarly informative to the original signal (Fig. 1D).

79 Several recent studies suggest that the complexity of brain activity is task-dependent, whereby
80 simpler tasks with lower cognitive demands are reflected by simpler and more compressible brain
81 activity patterns, and more complex tasks with higher cognitive demands are reflected by more
82 complex and less compressible brain activity patterns (Mack et al., 2020; Owen et al., 2021). These
83 findings complement other work suggesting that functional connectivity (correlation) patterns are
84 task-dependent (Finn et al., 2017; Owen et al., 2020; Cole et al., 2014), although see Gratton et
85 al. (2018). Higher-order cognitive processing of a common stimulus also appears to drive more
86 stereotyped task-related activity and functional connectivity across individuals (Hasson et al.,
87 2008; Lerner et al., 2011; Simony & Chang, 2020; Simony et al., 2016).

88 The above studies are consistent with two potential descriptions of how cognitive processes are

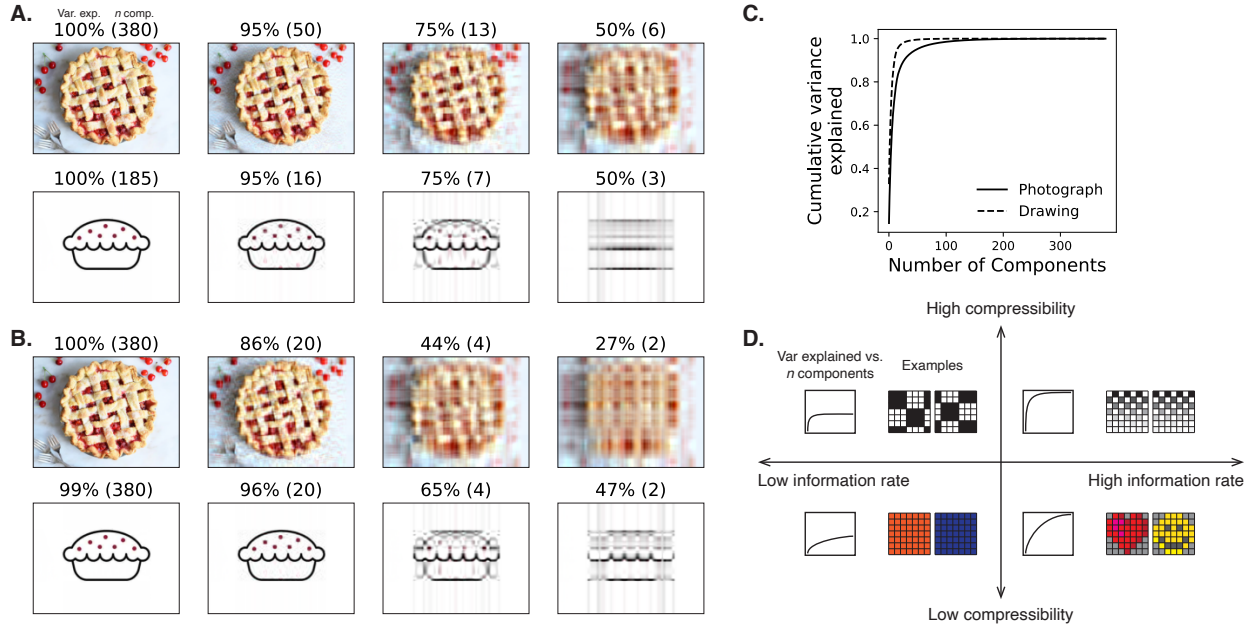


Figure 1: Information content and compressibility. **A. Variance explained for two images.** We applied principal components analysis to a photograph and drawing, treating each row of the images as “observations.” Across columns, we identified the number of components required to explain 100%, 95%, 75%, or 50% of the cumulative variance in each image (the 100% columns denote the original images). The numbers of components are indicated in parentheses, and the resulting “compressed” images are displayed. **B. Representing two images with different numbers of components.** Using the same principal component decompositions as in Panel A, we computed the cumulative proportion of variance explained with 380 (original images), 20, 4, or 2 components. **C. Cumulative variance explained versus number of components.** For the images displayed in Panels A and B, we plot the cumulative proportion of variance explained as a function of the number of components used to represent each image. **D. Information rate and compressibility.** Across multiple images, the information rate (i.e., the amount of information contained in each image; horizontal axis) is high when each individual pixel provides information that cannot be inferred from other pixels. High-information rate images tend to be high-resolution, and low-information rate images tend to be low-resolution. Compressibility is related to the difference between the information required to specify the original versus compressed images (vertical axis). Highly compressible images often contain predictable structure (redundancies) that can be leveraged to represent the images much more efficiently than in their original feature spaces.

89 reflects in brain activity patterns. One possibility is that the information rate of brain activity in-
90 creases during more complex or higher-level cognitive processing. If so, then the ability to reliably
91 decode cognitive states from brain activity patterns should improve with task complexity or with
92 the level (or “depth”) of cognitive processing. A second possibility is that the compressibility of
93 brain activity patterns increases during more complex or higher-level cognitive processing. If so,
94 then individual features of brain recordings, or compressed representations of brain recordings,
95 should carry more information during complex or high-level (versus simple or low-level) cognitive
96 tasks.

97 We used a previously collected neuroimaging dataset to estimate the extent to which each of
98 these two possibilities might hold. The dataset we examined comprised functional magnetic reso-
99 nance imaging (fMRI) data collected as participants listened to an audio recording of a 10-minute
100 story, temporally scrambled recordings of the story, or underwent a resting state scan (Simony
101 et al., 2016). Each of these experimental conditions evokes different depths of cognitive process-
102 ing (Simony et al., 2016; Lerner et al., 2011; Hasson et al., 2008; Owen et al., 2021). We used
103 across-participant classifiers to decode listening times in each condition, as a proxy for how “in-
104 formative” the task-specific activity patterns were (Simony & Chang, 2020). We also use principle
105 components analysis to generate lower-dimensional representations of the activity patterns. We
106 then repeated the classification analyses after preserving different numbers of components and
107 examined how classification accuracy changed across the different experimental conditions.

108 Results

109 We sought to understand whether higher-level cognition is reflected by more reliable and in-
110 formative brain activity patterns, and how compressibility of brain activity patterns relates to
111 cognitive complexity. We developed a computational framework for systematically assessing the
112 informativeness and compressibility of brain activity patterns recorded under different cognitive
113 circumstances. We used across-participant decoding accuracy (see *Forward inference and decoding*
114 *accuracy*) as a proxy for informativeness. To estimate the compressibility of the brain patterns, we
115 used group principal components analysis (PCA) to project the brain patterns into k -dimensional
116 spaces, for different values of k (see *Hierarchical Topographic Factor Analysis (HTFA)* and *Principal*

117 components analysis (PCA)). For more compressible brain patterns, decoding accuracy should be
118 more robust to small values of k .

119 We analyzed a dataset collected by Simony et al. (2016) that comprised four experimental
120 conditions. These conditions exposed participants to stimuli that systematically varied in cognitive
121 engagement. In the *intact* experimental condition, participants listened to an audio recording of
122 a 10-minute story. In the *paragraph*-scrambled experimental condition, participants listened to a
123 temporally scrambled version of the story, where the paragraphs occurred out of order, but where
124 the same set of paragraphs was presented over the entire listening interval. All participants in
125 this condition experienced the scrambled paragraphs in the same order. In the *word*-scrambled
126 experimental condition, participants listened to a temporally scrambled version of the story, where
127 the words occurred in a random order. Again, all participants in this condition experienced the
128 scrambled words in the same order. Finally, in the *rest* experimental condition, participants lay
129 in the scanner with no overt stimulus, while keeping their eyes open and blinking as needed.
130 This public dataset provided a convenient means for testing our hypothesis that different levels
131 of cognitive processing and engagement affect how informative and compressible the associated
132 brain patterns are.

133 To evaluate the relation between informativeness and compression for brain activity from each
134 experimental condition, we trained a series of across-participant temporal decoders on compressed
135 representations of the data. Figure 2A displays the decoding accuracy as a function of the number
136 of principal components used to represent the data. Several patterns were revealed by the analysis.
137 First, in general (i.e., across experimental conditions), decoding accuracy improves as the number
138 of components increases. However, decoding accuracy peaked at a higher level for experimental
139 conditions that exposed participants to cognitively richer stimuli. The peak decoding accuracy
140 was highest for the “intact” condition (versus paragraph: $t(\text{XXX}) = \text{XXX}, p = \text{XXX}$; versus word:
141 $t(\text{XXX}) = \text{XXX}, p = \text{XXX}$; versus rest: $t(\text{XXX}) = \text{XXX}, p = \text{XXX}$), next highest for the “paragraph”
142 condition (versus word: $t(\text{XXX}) = \text{XXX}, p = \text{XXX}$; versus rest: $t(\text{XXX}) = \text{XXX}, p = \text{XXX}$), and next
143 highest for the “word” condition (versus rest: $t(\text{XXX}) = \text{XXX}, p = \text{XXX}$). This ordering implies
144 that cognitively richer conditions evoke more stable brain activity patterns across people.

145 The cognitively richer conditions also displayed steeper initial slopes. For example, the intact
146 condition decoders reached an arbitrarily chosen threshold of 5% accuracy using fewer components

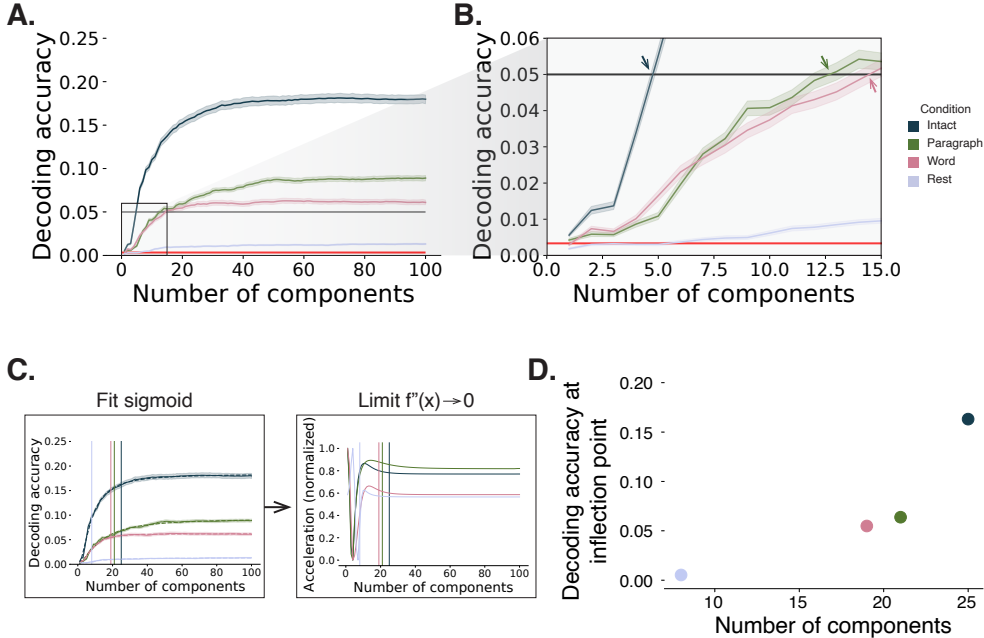


Figure 2: Decoding accuracy and compression. **A. Decoding accuracy by number of components.** Ribbons of each color display cross-validated decoding performance for each condition (intact, paragraph, word, and rest), as a function of the number of components (features) used to represent the data. The horizontal red line denotes chance performance, and the horizontal black line denotes 5% decoding accuracy (used as a reference in Panel B). **B. Numbers of components required to reach a fixed decoding accuracy threshold, by condition.** The panel displays a zoomed-in view of the inset in Panel A. Intersections between each condition’s decoding accuracy curve and the 5% decoding accuracy reference line are marked by arrows. **C. Estimating inflection points.** We sought to identify an “inflection point” for each decoding curve, denoting the number of components at which the decoding curve asymptotes. We fit sigmoid functions to each decoding curve (left sub-panel) and then computed the minimum number of components where the second derivative of the sigmoid was both positive and less than a threshold value of 0.0001. **D. Inflection points by condition.** Each dot displays the number of components (x -axis) and decoding accuracy (y -axis) at one condition’s inflection point. All error ribbons denote bootstrap-estimated 95% confidence intervals.

147 than the paragraph condition decoders ($t(\text{XXX}) = \text{XXX}, p = \text{XXX}$) or word condition decoders
148 ($t(\text{XXX}) = \text{XXX}, p = \text{XXX}$), and decoding accuracy never exceeded 5% for the rest condition. This
149 suggests that brain activity patterns evoked by cognitively richer conditions are more compressible,
150 such that representing the data using the same number of principal components provides more
151 information to the temporal decoders (Fig. 2B).

152 In every experimental condition, decoding accuracy appeared to asymptote (i.e., hit an upper
153 limit) beyond some characteristic number of components that differed across conditions. To
154 quantify the “inflection points” at which the decoding curves in Figure 2A flattened out, we fit a
155 sigmoid function to the average decoding curve for each condition. We defined the inflection point
156 for each condition as the point on the fitted sigmoid where the second derivative was both positive
157 and less than a threshold value of 0.0001 (i.e., approaching 0 from the right). These inflection
158 points reflect a “balance” between higher decoding accuracy (which tends to be better when
159 more components are used) and compression (which is better for fewer components). Plotting
160 each condition’s inflection point (Fig. 2D) reveals that both the number of components and the
161 decoding accuracy at each inflection point increase systematically across conditions in proportion
162 to cognitive richness.

163 If informativeness (to the temporal decoders) and compressibility vary with the cognitive
164 richness of the stimulus, might these measures also vary over time *within* a given condition? For
165 example, participants in the intact condition might process the ongoing story more deeply later
166 on in the story (compared with earlier in the story) given the additional narrative background
167 and context they had been exposed to by that point. To examine this possibility, we divided
168 each condition into three successive time segments. We computed decoding curves (Fig. 3A)
169 and inflection points (Fig. 3B) for each segment and condition. We found that, in the two most
170 cognitively rich conditions (intact and paragraph), both decoding accuracy and compressibility,
171 as reflected by the change in decoding curves, increased with listening time (intact: $t(\text{XXX}) =$
172 $\text{XXX}, p = \text{XXX}$; paragraph: $t(\text{XXX}) = \text{XXX}, p = \text{XXX}$). These changes may reflect an increase in
173 comprehension or depth of processing with listening time. In contrast, the decoding accuracy and
174 compressibility *decreased* with listening time in the word condition ($t(\text{XXX}) = \text{XXX}, p = \text{XXX}$) and
175 rest condition ($t(\text{XXX}) = \text{XXX}, p = \text{XXX}$). This might reflect the depletion of attentional resources
176 in the less-engaging word and rest conditions.

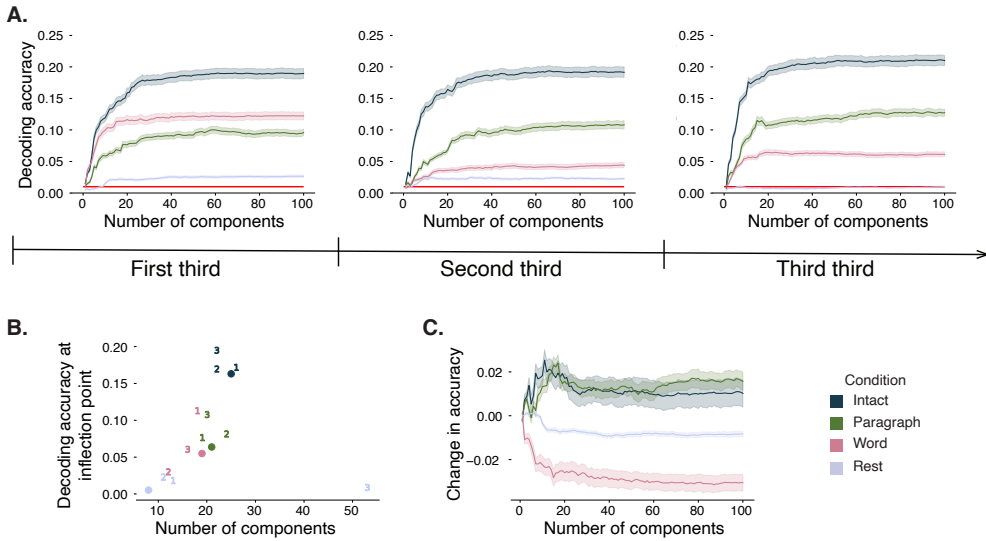


Figure 3: Changes in decoding accuracy and compression over time. **A. Decoding accuracy by number of components, by story segment.** Each family of curves is plotted in the same format as Figure 2A but reflects data only from one third of the dataset. **B. Inflection points by condition and segment.** The dots re-plot the inflection points from Figure 2D for reference. The numbers denote the inflection points for each third of the dataset (1: first third; 2: second third; 3: third third; colors denote experimental conditions). **C. Change in decoding accuracy over time, by number of components.** For each number of components (x-axis) and condition (color), we fit a regression line to the decoding accuracies obtained for the first, second, and third thirds of the dataset (corresponding to the left, middle, and right columns of Panel A, respectively). The y-axis denotes the slopes of the regression lines. All error ribbons denote bootstrap-estimated 95% confidence intervals.

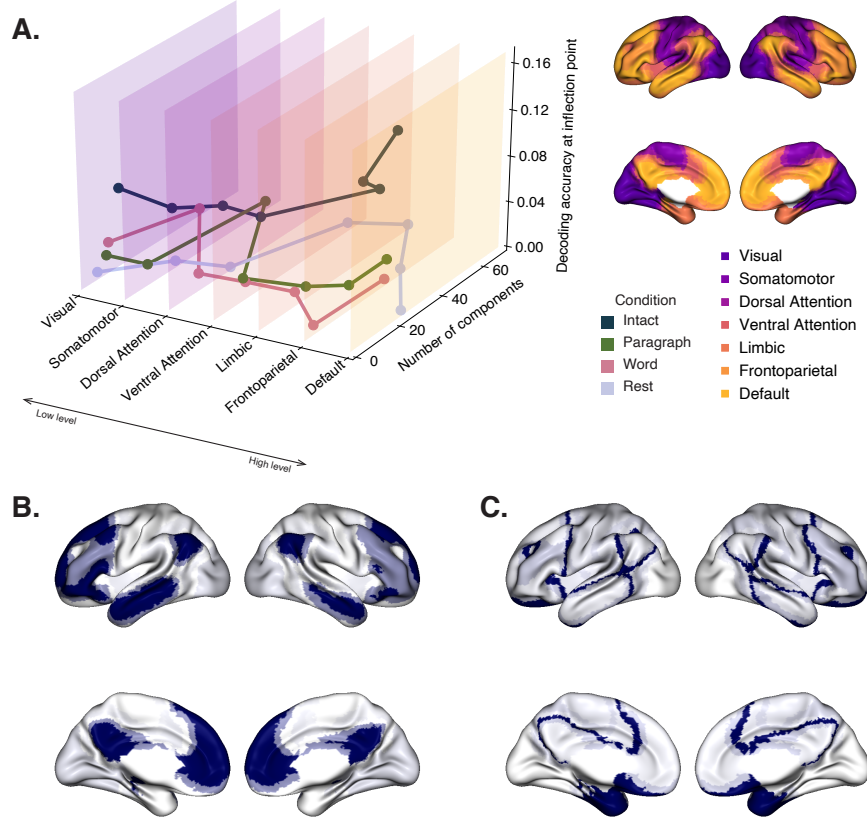


Figure 4: Network-specific decoding accuracy and compression. **A. Decoding accuracy and number of components for network-specific inflection points.** We considered the seven networks identified by Yeo et al. (2011). We computed each network’s inflection point, for each experimental condition, using the procedure described in Figure 2C. **B. Network-specific decoding accuracy.** Each of the seven networks are colored according to the decoding accuracy at the network’s inflection point for the “intact” experimental condition (corresponding to the dark blue curve in Panel A). **C. Network-specific compression.** Each of the seven networks are colored according to the number of components at the network’s inflection point for the intact experimental condition. Larger numbers of components reflect lower compressibility.

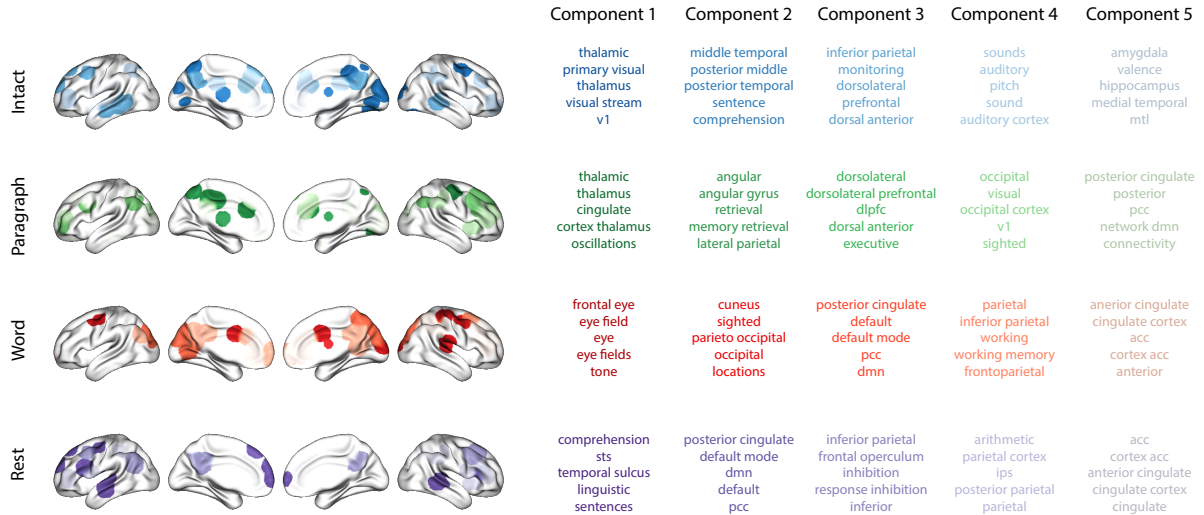


Figure 5: Top terms associated with the highest-weighted components by condition. Each row corresponds to an experimental condition, and the colors correspond to the component number (ranked by proportion of variance explained). The inflated brain plots display the top 20 highest-weighted hubs (see *Topographic Factor Analysis*) for each components'. The lists on the right display the top five Neurosynth terms (Rubin et al., 2017) decoded from each components' brain map. Analogous maps computed separately for each story segment may be found in Figure S1.

177 We also wondered how informativeness and compressibility in the different experimental
 178 conditions might vary across brain networks. We used a network parcellation identified by
 179 Yeo et al. (2011) to segment the brain into seven distinct networks. The networks can be sorted
 180 (roughly) in order from lower-level to higher-level cortex as follows (Fig. 4A): visual, somatomotor,
 181 dorsal attention, ventral attention, limbic, frontoparietal, and default mode. Next, we computed
 182 decoding curves separately for the activity patterns within each network and identified each
 183 network's inflection point, for each experimental condition. Moving from low-order networks
 184 to higher-order networks, we found that decoding accuracy (for the intact condition) tended to
 185 increase (Figs. 4B, S2). This suggests that higher-order networks may carry more content-relevant
 186 or stimulus-driven "information." We found no clear trends in the numbers of components at each
 187 network's inflection point across networks or conditions (Figs. 4C, S3). **JRM NOTE: expand on**
 188 **this once we have the new figures.**

189 In addition to examining different networks in isolation, we wondered about the general
 190 structure of the full-brain (i.e., potentially multi-network) activity patterns reflected by different
 191 principal components across different experimental conditions. Figure 5 displays inflated brain

maps of the top five highest-weighted components, for each experimental condition. We also used Neurosynth (Rubin et al., 2017) to identify, for each component, the top five terms associated with each map (see *Reverse inference*). We noticed (by inspection) several common themes across the sets of terms associated with each component and condition. Memory-related components included terms like “middle temporal,” “memory retrieval,” and “working memory.” Sensory processing related components included terms like “primary visual,” “auditory cortex,” “v1,” and so on. Other components were associated with sensory integration (e.g., “thalamic,” “cingulate,” etc.), sentence comprehension (e.g., “sentence,” “comprehension”), emotion and valence (e.g., “amygdala,” “valance”), or the default mode network (e.g., “default mode”). The components we identified were relatively stable across story segments (Fig. S1).

Discussion

We examined fMRI data collected as participants listened to an auditory recording of a story, scrambled recordings of the story, or underwent a resting state scan. We found that cognitively richer stimuli evoked more reliable (i.e., consistent across people) and information rich brain activity patterns. The brain patterns are also more compressible, in that each individual component provided more “signal” to temporal decoders relative to components of data from less cognitively rich conditions (Fig. 2). Over time (e.g., as the experiment progressed), these phenomena were strengthened. Specifically, across story segments, data from more cognitively rich conditions became more informative and compressible, and data from less cognitively rich conditions became less informative and compressible (Fig. 3). We also repeated these analyses separately for different brain networks. We found that networks traditionally associated with higher-level cognitive functions tended to provide more informative brain patterns than networks traditionally associated with lower level cognitive functions (Fig. 4). Finally, we examined the most dominant components of the brain activity patterns from each experimental condition. We used a reverse inference approach (Rubin et al., 2017) to identify the terms in the neuroimaging literature most commonly associated with the corresponding maps. As summarized in Figure 6, we found that terms associated with memory and sensory processing were associated with the strongest components in all three story listening conditions. Terms associated with sensory integration were associated with

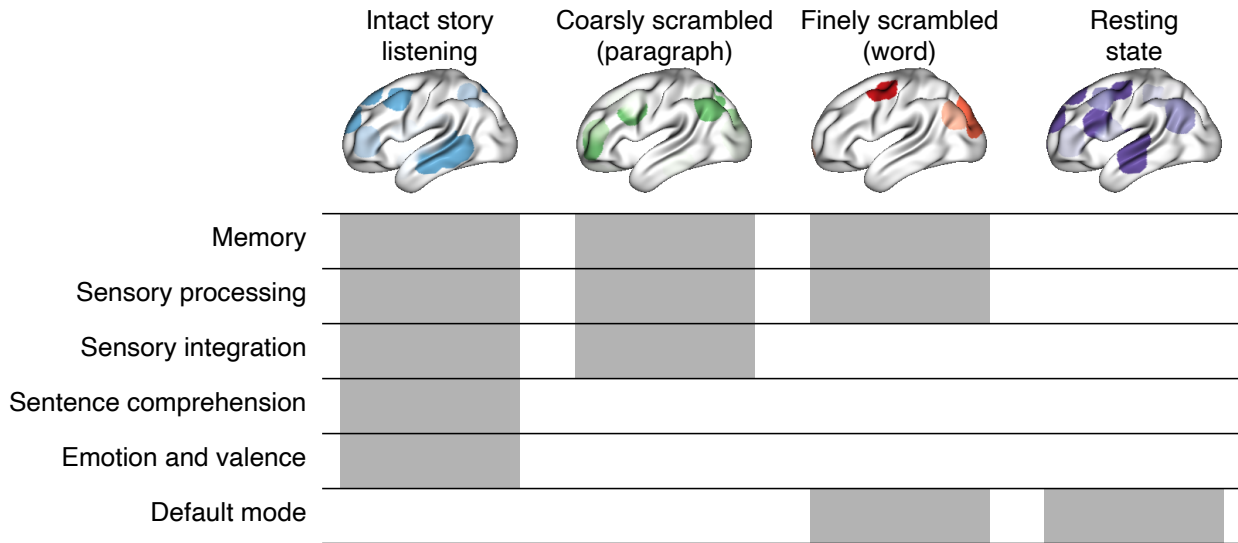


Figure 6: Summary of functions associated with top-weighted components by condition. Each column corresponds to an experimental condition. Brain maps in the top row are reproduced from Figure 5, for reference. Cognitive functions summarized from the top Neurosynth-derived terms in Figure 5 are listed in the rows on the left. Shaded cells denote which experimental conditions were associated with one or more top-weighted principal components associated with the given function.

220 the strongest components in the intact and paragraph-scrambled conditions. Terms associated with
 221 sentence comprehension, emotion, and valence were associated with the strongest components in
 222 the intact condition. Finally, terms associated with the default mode network were associated with
 223 the strongest components in the word-scrambled and resting state conditions. Taken together, our
 224 findings indicate that the informativeness and compressibility of our brain activity patterns are
 225 task-dependent, and these properties change systematically with factors like cognitive richness
 226 and depth of processing.

227 Methods

228 We measured properties of recorded neuroimaging data under different task conditions that varied
 229 systematically in cognitive engagement and depth of processing. We were especially interested in
 230 how *informative* and *compressible* the activity patterns were under these different conditions (Fig. 1).

231 **Functional neuroimaging data collected during story listening**

232 We examined an fMRI dataset collected by Simony et al. (2016) that the authors have made publicly
233 available at arks.princeton.edu/ark:/88435/dsp015d86p269k. The dataset comprises neuroimaging
234 data collected as participants listened to an audio recording of a story (intact condition; 36 par-
235 ticipants), listened to temporally scrambled recordings of the same story (17 participants in the
236 paragraph-scrambled condition listened to the paragraphs in a randomized order and 36 in the
237 word-scrambled condition listened to the words in a randomized order), or lay resting with their
238 eyes open in the scanner (rest condition; 36 participants). Full neuroimaging details may be found
239 in the original paper for which the data were collected Simony et al. (2016). Procedures were
240 approved by the Princeton University Committee on Activities Involving Human Subjects, and by
241 the Western Institutional Review Board (Puyallup, WA). All subjects were native English speakers
242 with normal hearing and provided written informed consent.

243 **Hierarchical topographic factor analysis (HTFA)**

244 Following our prior related work, we used HTFA Manning et al. (2018) to derive a compact
245 representation of the neuroimaging data. In brief, this approach approximates the timeseries
246 of voxel activations (44,415 voxels) using a much smaller number of radial basis function (RBF)
247 nodes (in this case, 700 nodes, as determined by an optimization procedure; Manning et al., 2018)).
248 This provides a convenient representation for examining full-brain activity patterns and network
249 dynamics. All of the analyses we carried out on the neuroimaging dataset were performed in this
250 lower-dimensional space. In other words, each participant's data matrix, \mathbf{X} , was a number-of-
251 timepoints (T) by 700 matrix of HTFA-derived factor weights (where the row and column labels
252 were matched across participants). Code for carrying out HTFA on fMRI data may be found as
253 part of the BrainIAK toolbox Capota et al. (2017); Kumar et al. (2021), which may be downloaded
254 at brainiak.org.

255 **Principal components analysis (PCA)**

256 We applied group PCA (Smith et al., 2014) separately to the HTFA-derived representations of the
257 data (i.e., factor loadings) from each experimental condition. Specifically, for each condition, we

258 considered the set of all participants' T by 700 factor weight matrices. We used group PCA to
259 project these 700-dimensional matrices into a series of k -dimensional spaces, for $k \in \{3, 4, 5, \dots, 700\}$.
260 This yielded a set of number-of-participants matrices, each with T rows and k columns.

261 **Temporal decoding**

262 We sought to identify neural patterns that reflected participants' ongoing cognitive processing of
263 incoming stimulus information. As reviewed by Simony et al. (2016), one way of homing in on
264 these stimulus-driven neural patterns is to compare activity patterns across individuals. In partic-
265 ular, neural patterns will be similar across individuals to the extent that the neural patterns under
266 consideration are stimulus-driven, and to the extent that the corresponding cognitive representa-
267 tions are reflected in similar spatial patterns across people Simony & Chang (2020). Following this
268 logic, we used an across-participant temporal decoding test developed by Manning et al. (2018) to
269 assess the degree to which different neural patterns reflected ongoing stimulus-driven cognitive
270 processing across people. The approach entails using a subset of the data to train a classifier to
271 decode stimulus timepoints (i.e., moments in the story participants listened to) from neural pat-
272 terns. We use decoding (forward inference) accuracy on held-out data, from held-out participants,
273 as a proxy for the extent to which the inputted neural patterns reflected stimulus-driven cognitive
274 processing in a similar way across individuals.

275 **Forward inference and decoding accuracy**

276 We used an across-participant correlation-based classifier to decode which stimulus timepoint
277 matched each timepoint's neural pattern. For a given value of k (i.e., number of principal com-
278 ponents), we first used group PCA to project the data from each condition into a k -dimensional
279 space. Next, we divided the participants into two groups: a template group, $\mathcal{G}_{\text{template}}$ (i.e., training
280 data), and a to-be-decoded group, $\mathcal{G}_{\text{decode}}$ (i.e., test data). We averaged the projected data within
281 each group to obtain a single T by k matrix for each group. Next, we correlated the rows of the two
282 averaged matrices to form a T by T decoding matrix, Λ . In this way, the rows of Λ reflected time-
283 points from the template group, while the columns reflected timepoints from the to-be-decoded
284 group. We used Λ to assign temporal labels to each timepoint (row) from the test group's ma-

285 trix, using the row of the training group’s matrix with which it was most highly correlated. We
286 repeated this decoding procedure, but using $\mathcal{G}_{\text{decode}}$ as the template group and $\mathcal{G}_{\text{template}}$ as the
287 to-be-decoded group. Given the true timepoint labels (for each group), we defined the decoding
288 accuracy as the average proportion of correctly decoded timepoints, across both groups (where
289 chance performance is $\frac{1}{T}$). In Figures 2 and 3 we report the decoding accuracy for each condition
290 and value of k , averaged across $n = 100$ cross validation folds.

291 **Reverse inference**

292 To help interpret the brain activity patterns we found within the contexts of other studies, we
293 created summary maps of each principal component, for each experimental condition, by summing
294 together the 20 HTFA-derived RBF nodes (see *Hierarchical Topographic Factor Analysis*) with the
295 highest absolute value weights for each of the top 5 components (Figs. 5, S1). We then carried
296 out a meta analysis using Neurosynth Rubin et al. (2017) to identify the 5 terms most commonly
297 associated with the given map.

298 **Data and code availability**

299 All of the code used to produce the figures and results in this manuscript, along with links to the
300 corresponding datasets, may be found at github.com/ContextLab/pca_paper.

301 **Acknowledgements**

302 We acknowledge discussions with Rick Betzel, Emily Finn, and Jim Haxby. Our work was sup-
303 ported in part by NSF CAREER Award Number 2145172 to J.R.M. The content is solely the re-
304 sponsibility of the authors and does not necessarily represent the official views of our supporting
305 organizations. The funders had no role in study design, data collection and analysis, decision to
306 publish, or preparation of the manuscript.

307 **Author contributions**

308 Conceptualization: J.R.M. and L.L.W.O. Methodology: J.R.M. and L.L.W.O. Implementation: L.L.W.O.
309 Analysis: L.L.W.O. Writing, Reviewing, and Editing: J.R.M. and L.L.W.O. Supervision: J.R.M.

310 **References**

- 311 Alvarez, S. A. (2002). *An exact analytical relation among recall, precision, and classification accuracy in*
312 *information retrieval* (Technical Report No. BCCS-02-01). Boston College.
- 313 Capota, M., Turek, J., Chen, P.-H., Zhu, X., Manning, J. R., Sundaram, N., ... Shin, Y. S. (2017).
314 *Brain imaging analysis kit.*
- 315 Cole, M. W., Bassett, D. S., Power, J. D., Braver, T. S., & Petersen, S. E. (2014). Intrinsic and
316 task-evoked network architectures of the human brain. *Neuron*, 83(1), 238–251.
- 317 Finn, E. S., Scheinost, D., Finn, D. M., Shen, X., Papademetris, X., & Constable, R. T. (2017).
318 Can brain state be manipulated to emphasize individual differences in functional connectivity.
319 *NeuroImage*, 160, 140–151.
- 320 Finn, E. S., Shen, X., Scheinost, D., Rosenberg, M. D., Huang, J., Chun, M. M., ... Constable, R. T.
321 (2015). Functional connectome fingerprinting: identifying individuals using patterns of brain
322 connectivity. *Nature Neuroscience*, 18, 1664–1671.
- 323 Glerean, E., Salmi, J., Lahnakoski, J. M., Jääskeläinen, I. P., & Sams, M. (2012). Functional magnetic
324 resonance imaging phase synchronization as a measure of dynamic functional connectivity.
325 *Brain Connectivity*, 2(2), 91–101.
- 326 Gratton, C., Laumann, T. O., Nielsen, A. N., Greene, D. J., Gordon, E. M., Gilmore, A. W., ...
327 Petersen, S. E. (2018). Functional brain networks are dominated by stable group and individual
328 factors, not cognitive or daily variation. *Neuron*, 98(2), 439–452.
- 329 Hasson, U., Yang, E., Vallines, I., Heeger, D. J., & Rubin, N. (2008). A hierarchy of temporal
330 receptive windows in human cortex. *The Journal of Neuroscience*, 28(10), 2539–2550.

- 331 Kumar, M., Anderson, M. J., Antony, J. W., Baldassano, C., Brooks, P. P., Cai, M. B., ... Norman,
332 K. A. (2021). BrainIAK: the brain image analysis kit. *Aperture*, *In press*.
- 333 Lerner, Y., Honey, C. J., Silbert, L. J., & Hasson, U. (2011). Topographic mapping of a hierarchy of
334 temporal receptive windows using a narrated story. *The Journal of Neuroscience*, 31(8), 2906–2915.
- 335 Mack, M. L., Preston, A. R., & Love, B. C. (2020). Ventromedial prefrontal cortex compression during
336 concept learning. *Nature Communications*, 11(46), doi.org/10.1038/s41467-019-13930-8.
- 337 Manning, J. R., Zhu, X., Willke, T. L., Ranganath, R., Stachenfeld, K., Hasson, U., ... Norman,
338 K. A. (2018). A probabilistic approach to discovering dynamic full-brain functional connectivity patterns. *NeuroImage*, 180, 243–252.
- 340 Norman, K. A., Polyn, S. M., Detre, G. J., & Haxby, J. V. (2006). Beyond mind-reading: multi-voxel
341 pattern analysis of fMRI data. *Trends in Cognitive Sciences*, 10(9), 424–430.
- 342 Owen, L. L. W., Chang, T. H., & Manning, J. R. (2021). High-level cognition during story listening is
343 reflected in high-order dynamic correlations in neural activity patterns. *Nature Communications*,
344 12(5728), doi.org/10.1038/s41467-021-25876-x.
- 345 Owen, L. L. W., Muntianu, T. A., Heusser, A. C., Daly, P., Scangos, K. W., & Manning, J. R. (2020). A
346 Gaussian process model of human electrocorticographic data. *Cerebral Cortex*, 30(10), 5333–5345.
- 347 Rubin, T. N., Kyoejo, O., Gorgolewski, K. J., Jones, M. N., Poldrack, R. A., & Yarkoni, T. (2017).
348 Decoding brain activity using a large-scale probabilistic functional-anatomical atlas of human
349 cognition. *PLoS Computational Biology*, 13(10), e1005649.
- 350 Scangos, K. W., Khambhati, A. N., Daly, P. M., Owen, L. L. W., Manning, J. R., Ambrose, J. B.,
351 ... Chang, E. F. (2021). Biomarkers of depression symptoms defined by direct intracranial
352 neurophysiology. *Frontiers in Human Neuroscience*, *In press*.
- 353 Shannon, C. E. (1948). A mathematical theory of communication. *Bell System Technical Journal*,
354 27(3), 379–423.
- 355 Simony, E., & Chang, C. (2020). Analysis of stimulus-induced brain dynamics during naturalistic
356 paradigms. *NeuroImage*, 216, 116461.

- 357 Simony, E., Honey, C. J., Chen, J., & Hasson, U. (2016). Dynamic reconfiguration of the default
358 mode network during narrative comprehension. *Nature Communications*, 7(12141), 1–13.
- 359 Smith, S. M., Hyvärinen, A., Varoquaux, G., Miller, K. L., & Beckmann, C. F. (2014). Group-PCA
360 for very large fMRI datasets. *NeuroImage*, 101, 738–749.
- 361 Yeo, B. T. T., Krienen, F. M., Sepulcre, J., Sabuncu, M. R., Lashkari, D., Hollinshead, M., . . . Buckner,
362 R. L. (2011). The organization of the human cerebral cortex estimated by intrinsic functional
363 connectivity. *Journal of Neurophysiology*, 106(3), 1125–1165.